Received: 22 July 2020 | Revised: 25 August 2020 | Accepted: 14 September 2020

DOI: 10.1002/hbm.25213

Check for updates

RESEARCH ARTICLE

WILEY

Early red nucleus atrophy in relapse-onset multiple sclerosis

Monica Margoni[1,2] | Davide Poggiali[2,3] | Sofia Zywicki[1] | Martina Rubin[1] | Andrea Lazzarotto[1] | Silvia Franciotta[1] | Maria Giulia Anglani[4] | Francesco Causin[4] | Francesca Rinaldi[1] | Paola Perini[1] | Massimo Filippi[5,6,7,8] | Paolo Gallo[1,9]

[1]Multiple Sclerosis Centre of the Veneto Region (CeSMuV), University Hospital of Padua, Padua, Italy

[2]Padova Neuroscience Centre (PNC), University of Padua, Padua, Italy

[3]Department of Mathematics, University of Padua, Padua, Italy

[4]Neuroradiology Unit, University Hospital of Padua, Padua, Italy

[5]Neuroimaging Research Unit, Institute of Experimental Neurology, Division of Neuroscience, IRCCS San Raffaele Scientific Institute, Milan, Italy

[6]Neurology Unit, IRCCS San Raffaele Scientific Institute, Milan, Italy

[7]Neurophysiology Unit, IRCCS San Raffaele Scientific Institute, Milan, Italy

[8]Vita-Salute San Raffaele University, Milan, Italy

[9]Department of Neurosciences, Medical School, University of Padua, Padua, Italy

Correspondence
Monica Margoni, Multiple Sclerosis Centre of the Veneto Region, Padua Neuroscience Centre, University of Padua, Via Giustiniani 2, 35128 Padova, Italy.
Email: monica.margoni@phd.unipd.it

Abstract

No study has investigated red nucleus (RN) atrophy in multiple sclerosis (MS) despite cerebellum and its connections are elective sites of MS-related pathology. In this study, we explore RN atrophy in early MS phases and its association with cerebellar damage (focal lesions and atrophy) and physical disability. Thirty-seven relapse-onset MS (RMS) patients having mean age of 35.6 ± 8.5 (18–56) years and mean disease duration of 1.1 ± 1.5 (0–5) years, and 36 age- and sex-matched healthy controls (HC) were studied. Cerebellar and RN lesions and volumes were analyzed on 3 T-MRI images. RMS did not differ from HC in cerebellar lobe volumes but significantly differed in both right (107.84 ± 13.95 mm^3 vs. 99.37 ± 11.53 mm^3, $p = .019$) and left (109.71 ± 14.94 mm^3 vs. 100.47 ± 15.78 mm^3, $p = .020$) RN volumes. Cerebellar white matter lesion volume (WMLV) inversely correlated with both right and left RN volumes ($r = -.333$, $p = .004$ and $r = -.298$, $p = .010$, respectively), while no correlation was detected between RN volumes and mean cortical thickness, cerebellar gray matter lesion volume, and supratentorial WMLV (right RN: $r = -.147$, $p = .216$; left RN: $r = -.153$, $p = .196$). Right, but not left, RN volume inversely correlated with midbrain WMLV ($r = -.310$, $p = .008$), while no correlation was observed between whole brainstem WMLV and either RN volumes (right RN: $r = -.164$, $p = .164$; left RN: $r = -.64$, $p = .588$). Finally, left RN volume correlated with vermis VIIb ($r = .297$, $p = .011$) and right interposed nucleus ($r = .249$, $p = .034$) volumes. We observed RN atrophy in early RMS, likely resulting from anterograde axonal degeneration starting in cerebellar and midbrain WML. RN atrophy seems a promising marker of neurodegeneration and/or cerebellar damage in RMS.

KEYWORDS

cerebellum, MRI, red nucleus

This is an open access article under the terms of the Creative Commons Attribution License, which permits use, distribution and reproduction in any medium, provided the original work is properly cited.
© 2020 The Authors. *Human Brain Mapping* published by Wiley Periodicals LLC.

1 | INTRODUCTION

The red nucleus (RN), a large neuronal structure located in the most rostral part of ventral midbrain, owes its name to its high iron content, which makes it clearly identifiable both in fresh tissue sections and in T2-weighted magnetic resonance imaging (MRI) sequences. According to its cytoarchitecture, the RN is divided in a rostral parvocellular part (pRN), accounting for up to 80% of the nucleus volume and receiving inputs primarily from the nucleus dentatus, and a caudal magnocellular part (mRN, 20%) receiving inputs primarily from nucleus interpositus and nucleus emboliform (Massion, 1988; Onodera & Hicks, 2009; ten Donkelaar, 1988).

mRN and pRN have different functional roles. While mRN is involved in intra- and inter-limb coordination (Lavoie & Drew, 2002) and probably plays a role in compensating lesions of the corticospinal tract (Belhaj-Saif & Cheney, 2000; Siegel, Fink, Strittmatter, & Cafferty, 2015), pRN has been suggested to be involved in more complex functional networks, including those integrating cognitive-motor functions such as motor learning, error encoding, timing, and control of the ongoing movement (Habas, Guillevin, & Abanou, 2010; Lang et al., 2017; Reid et al., 2009). These observations further point out the association of specific cerebellar lobules with cognitive and affective functions (Koziol et al., 2014; Lazzarotto et al., 2020; Schmahmann & Sherman, 1997). Finally, worth of interest is also the possible role of cerebellar and RN damage in the early development of disabling multiple sclerosis (MS) symptoms such as fatigue and depression (Lazzarotto et al., 2020).

The cerebellum and the brainstem are major sites of pathology in MS and their involvement, although frequently asymptomatic, is known to be associated with a more severe prognosis (Damasceno, Von Glehn, Brandao, Damasceno, & Cendes, 2013; Tintore et al., 2010). Lesions damaging RN structure and connections may cause severe clinical picture, such as the rubral tremor (Koch, Mostert, Heersema, & De Keyser, 2007). Due to its major connections with the cerebellum, RN atrophy can result from trans-synaptic degeneration following cerebellar damage. Indeed, in a preclinical study in mutant mice, the loss of Purkinje cells was followed by the progressive atrophy of deep cerebellar nuclei due to anterograde trans-synaptic degeneration (Triarhou, Norton, & Ghetti, 1987).

Given these premises, we aimed to explore whether RN atrophy can be detected in the early disease phases, and whether this is associated with cerebral or cerebellar MRI metrics of white matter (WM) or gray matter (GM) damage, and early physical disability in relapse-onset MS (RMS) patients.

2 | MATERIALS AND METHODS

2.1 | Patients

Thirty-seven relapsing–remitting (RRMS) patients (mean age: 35.6 ± 8.5 years; range: 18–56 years; F/M: 25/12) who met the 2010 and 2017 diagnostic criteria (Polman et al., 2011; Thompson et al., 2018) were enrolled in this retrospective study. Thirty-six sex- and age-matched healthy controls (HC) (mean age: 33.8 ± 9.9 years; range: 23–63 years; F/M = 24/12) constituted the reference population.

All patients that were diagnosed to have MS in the period March 2014 to August 2018, were selected according to the following criteria: (a) age range, 18–65 years; (b) clinical disease duration <5 years; (c) no history/evidence of neurologic or psychiatric disorders other than MS; (d) no history of alcohol or drug abuse; (e) good quality of MRI (i.e., we excluded those with movement artifacts).

Each participant gave written informed consent and the study was approved by the local Ethics Committee, according to the IV revision of Declaration of Helsinki.

2.2 | Clinical assessment

All patients underwent a neurological examination, including Expanded Disability Status Scale (EDSS) (Kurtzke, 1983) within 1 week from the MRI acquisition.

2.3 | MRI data acquisition

MRI was obtained on a 3.0 T scanner (Ingenia, Philips Medical Systems, Best, The Netherlands) with 33 mT/m power gradient and a 32-channel head coil. No major hardware upgrades occurred during the study, and bimonthly quality assurance sessions assured measurement stability. The MRI protocol included the following sequences: (a) three-dimensional (3D) T1 TFE: repetition time (RT) = 7,2, echo time (ET) = 3,3, TFE factor 218; 165 contiguous axial slices with the off-center positioned on zero with thickness of 1.0 mm; flip angle = 9; matrix size = 220 × 218; FOV 240 × 240 × 181.5 mm; (b) 3D-FLAIR: RT = 4,800 ms, ET = 293 ms, inversion time (IT) = 1,650 ms; 331 contiguous axial slices with thickness of 1.0 mm; matrix size 220 × 217; and FOV = 240 × 240 × 182 mm; (c) 3D-DIR: RT = 5,500 ms, ET = 294 ms, inversion time (IT) = 2,550 ms; 281 contiguous axial slices with thickness of 1.0 mm; matrix size 208 × 209; and FOV = 250 × 250 × 168 mm.

2.4 | MRI data processing

Quantification of both WM lesion volume (WMLV) on FLAIR images and GM lesion volume (GMLV) on DIR images was performed in each patient by two experienced observers (SZ, MR), unaware of subject identity, employing a semiautomated segmentation technique (ITKSNAP).

Mean cortical thickness and intracranial volume (ICV) were obtained by applying the Freesurfer software on lesion-filled 3D-T1 weighted images (Fischl & Dale, 2000).

Cerebellar volumes were calculated on lesion-filled 3DT1-weighted images using the spatially unbiased infratentorial toolbox (SUIT) version 3.2, implemented in statistical parametric mapping 12 (SPM 12) (software: http://www.fil.ion. ucl.ac.uk/spm).

Cerebellum and brainstem were identified and isolated automatically, and a mask was automatically generated by calculating the

maximum of the probability of each voxel belonging to one of these structures. Each obtained mask was visually inspected. Next, the isolated cerebellum was aligned to the SUIT atlas template via an affine transformation (for the linear part of the normalization) and a nonlinear transformation using the diffeomorphic anatomical registration using Exponentiated Lie algebra (Avants et al., 2011). The individual cerebellum was therefore resliced in the atlas space, modulating in order to grant volume preservation (D'Ambrosio et al., 2017). Finally, by applying an inverse transformation matrix derived from the previous co-registration step, the SUIT atlas was aligned to the native subject space, and lobular volumes were calculated.

RN volumes were obtained from FLAIR images using a FLAIR template in MNI152 space, derived from a sex and age-matched healthy population. Priors probability images of RN, manually labeled on high resolution MRIs of a healthy population (n = 44, F/M = 21/23, mean age: 32.9, range: 18–60), were also employed (Winkler, Kochunov, & Glahn, n.d.; Ashburner & Friston, 2005; Keuken et al., 2014; Keuken et al., 2017; Kochunov et al., 2006).

FLAIR images were nonlinearly registered to the FLAIR template by means of ANTs registration tool (Avants, Epstein, Grossman, & Gee, 2008), and the inverse warp was applied to priors. From the so-obtained priors in patient's space, the posteriors probability images were computed by means of Atropos (Wang & Yushkevich, 2013) (Figure 1).

Two experienced investigators (MM, DP), blinded to clinical data, visually inspected all RN. Only in three cases the pipeline was re-run due to inconsistent segmentation.

3 | STATISTICAL ANALYSIS

Statistical analysis was performed using SPSS Statistics 23 (SPSS Chicago, Ilinois). A Shaphiro-Wilk test and visual analysis of histograms were used to test the normality of the data.

Student's t test was used to test group differences in term of age, χ^2 test was used to test possible differences in terms of sex.

Group differences in terms of cerebellar and RN volumes were tested via multivariate Generalized Linear Model (GLM), including ICV as a covariate of no interest to account for head size. Correlations between MRI metrics and clinical disability were explored with Spearman's rank correlation coefficient.

All p values were two-sided and considered statistically significant when $p < .05$. Since our study is exploratory, we did not adjust for multiple comparisons.

4 | RESULTS

4.1 | Clinical and MRI findings in RRMS and HC

RRMS and HC did not differ in age (p = .42) and sex (p = 1.0). At MRI scan, the patients had mean disease duration of 1.1 ± 1.5 years (range 0–5) and median EDSS score of 2.0 (interquartile range [IQR]: 1.5–2.0, range: 1.0–6.0). The median cerebellar, brainstem and pyramidal functional system (FS) scores were 0.0 (IQR 0.0–0.0; range: 0.0–2.0), 0.0 (IQR 0.0–0.0: range: 0.0–2.0) and 1.0 (IQR 1.0–1.0; range: 0.0–3.0), respectively.

RRMS had a mean supratentorial white matter lesion volume (WMLV) of 341.02 ± 1,172.80 mm^3, cerebellar WMLV of 123.13 ± 163.43 mm^3, brainstem WMLV of 85.08 ± 147.0 mm^3, midbrain WMLV of 25.13 ± 56.45 mm^3 and cortical gray matter lesion volume (GMLV) of 59.65 ± 214.43 mm^3. Mean cortical thickness did not differ between RRMS and HC (5.78 ± 0.27 mm vs. 5.87 ± 0.38 mm, p = .371).

Table 1 summarizes the main demographic, clinical and MRI characteristics of the groups.

4.2 | RN volume is decreased in RRMS compared with HC

Anterior and posterior cerebellar lobe volumes did not differ between MS patients and HC. Despite the very short disease duration, MS

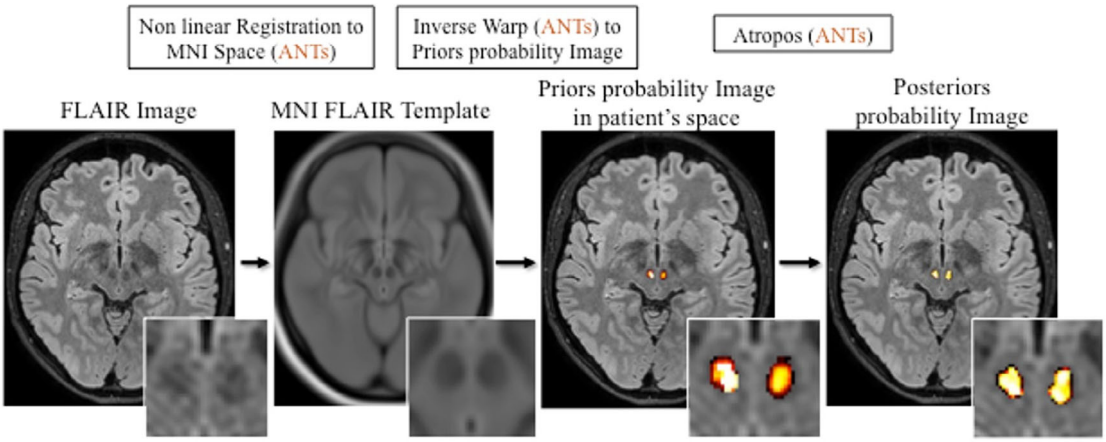


FIGURE 1 A schematic illustration of the processing pipeline to evaluate red nucleus volume (see Material and Methods for explanations)

TABLE 1 Demographic and clinical features of the groups included in the study

	HC (*n* = 36)	RRMS (*n* = 37)	*p**
Sex, F/M	24/12	25/12	1.0
Age at MRI scan, mean ± *SD* (years)	33.8 ± 9.9	35.6 ± 8.5	.42
Disease duration, mean ± *SD* (years)	–	1.1 ± 1.5	–
EDSS, median (IQR)	–	2.0 (1.5–2.0)	–
Right RN, mean ± *SD* (mm^3)	107.84 ± 13.95	99.37 ± 11.53	*.019* *
Left RN, mean ± *SD* (mm^3)	109.71 ± 14.94	100.47 ± 15.78	*.020* *
Mean cortical thickness (mm)	5.87 ± 0.38	5.78 ± 0.27	.371
Cerebellar WMLV, mean ± *SD* (mm^3)	–	123.13 ± 163.43	–
Supratentorial WMLV, mean ± *SD* (mm^3)	–	341.02 ± 1,172.80	–
Brainstem WMLV, mean ± *SD* (mm^3)	–	85.08 ± 147.0	–
Midbrain WMVL, mean ± *SD* (mm^3)	–	25.13 ± 56.45	–
Cortical GMLV, mean ± *SD* (mm^3)		59.65 ± 214.43	–

Abbreviations: EDSS, expanded disability status scale; GMLV, gray matter lesion volume; HC, healthy controls; IQR, interquartile range; RN, red nucleus; RRMS, relapsing–remitting multiple sclerosis; *SD*, standard deviation; WMLV, white matter lesion volume.
*$p < .05$.

patients had a significant reduction of both right ($p = .019$; 107.84 ± 13.95 mm^3 vs. 99.37 ± 11.53 mm^3) and left RN ($p = .020$; 109.71 ± 14.94 mm^3 vs. 100.47 ± 15.78 mm^3) volume compared with HC (Table 1). A complete list of the cerebellar volumetric analysis, with the respective *p* values, is reported in Table 2.

4.3 | RN volume correlates with cerebellar and midbrain WM lesions

A significant inverse correlation was found between cerebellar WMLV and both RN volumes (right: $r = -.333$, $p = .004$, and left: $r = -.298$, $p = .010$, respectively), while no correlation could be detected between RN volumes and mean cortical thickness (left RN: $r = .155$, $p = .190$; right RN: $r = .177$, $p = .134$), cerebellar GMLV (left RN: $r = -.125$, $p = .291$, right RN: $r = -.227$, $p = .053$) and supratentorial WMLV (right RN: $r = -.147$, $p = .216$; left RN: $r = -.153$, $p = .196$, respectively). Right, but not left, RN volume inversely correlated with midbrain WMLV ($r = -.310$, $p = .008$), while no correlation was observed between brainstem WMLV and either RN volumes (right RN: $r = -.164$, $p = .164$; left RN: $r = -.64$, $p = .588$).

4.4 | RN atrophy associates with cerebellar lobule atrophy and cerebellar function

Some low/moderate, but significant, correlations emerged between the volume of RN volume and that of some cerebellar lobules. Namely, the left RN volume correlated with vermis VIIb ($r = .297$, $p = .011$) and right interposed nucleus ($r = .249$, $p = .034$) volumes. Moreover, the right RN volume correlated with cerebellar FS score of EDSS ($r = -.360$, $p = .029$).

No correlation was found between RN volumes and disease duration (right RN: $r = -.318$, $p = .055$; left RN: $r = -.274$, $p = .101$) or EDSS score (right RN: $r = -.168$, $p = .444$; left RN: $r = -.09$, $p = .679$).

5 | DISCUSSION

Looking for early markers of neurodegeneration in RMS, we explored RN changes in a very early disease phase. Since the cerebellum and its connections are major sites of MS-related pathology (Parmar et al., 2018) and a pre-clinical study in Purkinje cell degeneration mutant mice disclosed trans-synaptic degeneration of deep cerebellar nuclei (Triarhou et al., 1987), our working hypothesis was that early RN atrophy could be the result of trans-synaptic anterograde axonal neurodegeneration starting in cerebellar WM and GM lesions.

We observed that RN volume in RMS, having very short disease duration (1.1 ± 1.5 years), was significantly lower compared with matched HC and correlated with cerebellar and midbrain WMLV, but not with supratentorial WMLV. Moreover, RN volume directly associated with the volume of some cerebellar lobules, but not with cerebellar GMLV. These observations suggest that RN atrophy could, at least partly, result from an axonal degeneration starting in cerebellum and midbrain WM lesions.

Our findings are particularly interesting on the light of previous observations in other neurological diseases. Indeed, RN volume was increased in patients with Parkinson's disease and significantly correlated with disease duration and severity, suggesting a compensatory activation of this nucleus (Colpan & Slavin, 2010), probably aimed at compensating the impaired function of the extra-pyramidal network. Moreover, in nonhuman primates (Philippens, Wubben, Franke, Hofman, & Langermans, 2019) larger RN volume inversely associated with the severity of extra-pyramidal symptoms. Finally, a damaged striato-thalamo-cortical pathway was found to result in a compensatory increase in RN activation (Philippens et al., 2019). All these observations suggest a compensatory function of RN in the presence of an extra-pyramidal disorder.

The RN seems to play a compensatory role even in patients with severe corticospinal tract injury following ischaemic stroke. Indeed, elevated levels of neuronal activity were observed in the RN of the affected hemisphere, especially in the early phases following stroke,

TABLE 2 Mean cerebellar volumes (mm^3) and *SD* of RRMS and healthy controls (HC)

	HC (*n* = 36)		RRMS (*n* = 37)		
	Mean	*SD*	Mean	*SD*	*p*
Left I-IV	0.002301502	0.000670027	0.002376645	0.000561846	.614
Right I-IV	0.002590352	0.000842328	0.002791260	0.000681491	.311
Left V	0.002919112	0.000872980	0.003009530	0.000723322	.628
Right V	0.002740069	0.000927967	0.002935002	0.000692913	.298
Left VI	0.006317410	0.002007192	0.006480943	0.001637477	.724
Vermis VI	0.001424024	0.000449293	0.001430352	0.000349973	.973
Right VI	0.005369853	0.001606742	0.005707507	0.001348242	.374
Left crus I	0.009709009	0.002741510	0.009378255	0.002320982	.512
Vermis crus I	1.06528E-05	5.61335E-06	1.10246E-05	6.81924E-06	1.000
Right crus I	0.008383129	0.002303089	0.008636830	0.001948583	.705
Left crus II	0.006719993	0.002055345	0.006909523	0.001895466	.769
Vermis crus II	0.000351424	0.000101609	0.000338894	8.20934E-05	.595
Right crus II	0.006164449	0.001827956	0.006507936	0.001707451	.487
Left VIIb	0.003326942	0.001027895	0.003502277	0.000866804	.455
Vermis VIIb	0.000160291	5.13925E-05	0.000150075	4.06692E-05	.480
Right VIIb	0.003379965	0.001037441	0.003513652	0.000856862	.564
Left VIIIa	0.003382789	0.001072485	0.003625168	0.000891045	.327
Vermis VIIIa	0.000891382	0.000258704	0.000861586	0.000186131	.558
Right VIIIa	0.003322524	0.001090567	0.003514819	0.000879843	.440
Left VIIIb	0.002637954	0.000846047	0.002854016	0.000777884	.274
Vermis VIIIb	0.000443174	0.000128391	0.000455487	9.50461E-05	.685
Right VIIIb	0.002931313	0.000941996	0.003119420	0.000791151	.390
Left IX	0.002375767	0.000705235	0.002399400	0.00059463	.771
Vermis IX	0.000560461	0.000139537	0.000567502	0.000113259	.773
Right IX	0.002854704	0.000838599	0.002868548	0.000646645	.878
Left X	0.000363149	0.000127645	0.000389401	0.000138833	.305
Vermis X	0.000275069	6.7564E-05	0.000292240	6.6236E-05	.211
Right X	0.000431827	0.000139280	0.000466224	0.000120889	.242
Left dentate	0.000568435	0.000125495	0.00057703	0.000115679	.660
Right dentate	0.000546634	0.000147238	0.000538615	0.000106714	.910
Left interposed	9.126E-06	3.7176E-06	8.17138E-06	3.23017E-06	.200
Right interposed	5.60918E-06	2.51593E-06	5.56481E-06	2.32856E-06	1.000

Note: p values were calculated with Generalized Linear Model; significance level was set at $p < .05$.

suggesting that RN could work as a compensatory structure to support the residual motor functions (Yeo & Jang, 2010). Microstructural RN changes, reflecting plastic and functional remodeling and associated with better motor function recovery, have been confirmed in other studies (Takenobu et al., 2014).

The above-summarized findings in Parkinson's disease and stroke strongly differ from our observations. Indeed, while direct pyramidal and extra-pyramidal damages are followed by a compensatory reaction of the RN, cerebellar damage associates with its atrophy. Thus, the initial RN atrophy observed in early RMS phases, may be considered a potential MRI marker of neurodegeneration following cerebellar damage and merits to be further investigated as negative prognostic factor. Indeed, the early NR atrophy might impair its potential functional compensatory role in case of corticospinal damage, that is, one of the major determinants of disability in MS.

Our data are in line with the increasing evidence of atrophy of deep gray matter nuclei in early RMS stages (Eshaghi et al., 2018), which indicates that this MRI metric may have a prognostic value since it associates with an increased risk of EDSS progression (Eshaghi et al., 2018) and cognitive decline in a relative shorter time (Riccitelli et al., 2011; Schoonheim et al., 2015). Interestingly, we also found an inverse association between RN atrophy and the cerebellar FS score of EDSS, suggesting that NR atrophy may be a specific marker of cerebellar damage rather than a generic marker of diffuse neurodegeneration.

The initial and significant, although slight correlations between RN atrophy and some cerebellar lobule atrophy indicates that the loss of volumes of these structures may proceed in parallel, probably as a

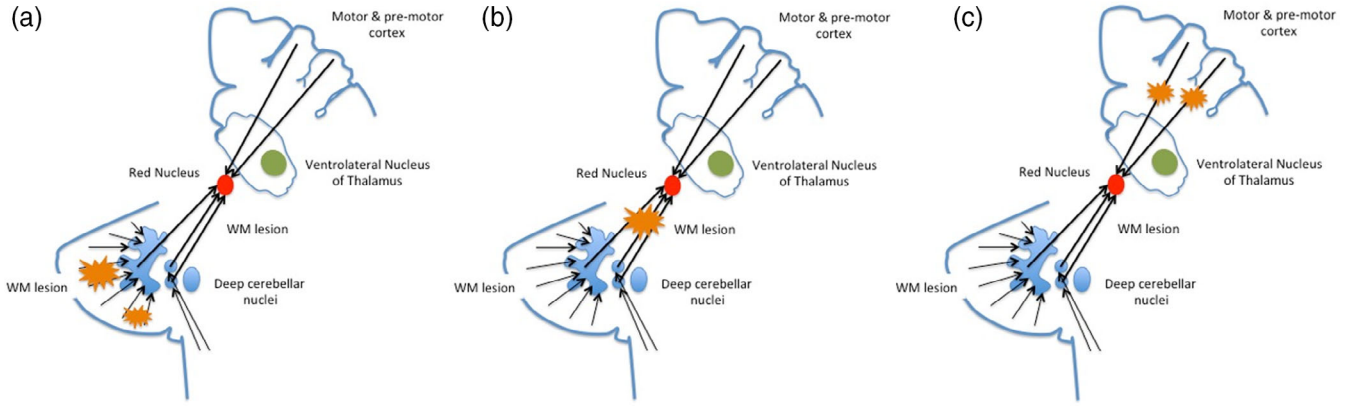


FIGURE 2 Possible causes of anterograde trans-synaptic degeneration of red nucleus (RN) RMS: (a) lesions in the cerebellar subcortical white matter (WM); (b) WM damage between the cerebellar nuclei and RN (i.e., superior cerebellar peduncle); (c) WM damage of the cortical-rubral trait

consequence of retrograde and trans-synaptic anterograde axonal degenerations starting in cerebellar WM lesions (Figure 2). Consequently, we may argue that RN atrophy could also reflect cerebellar pathology in normal appearing cerebellar white and gray matter, not detectable by conventional MRI sequences.

We are aware of the major limitation of our explorative study, namely, the relative low number of patients analyzed. However, we would like to further point out the single center and blind setting of our study, that make our data homogeneous and reliable. Moreover, we are also aware that only longitudinal studies may help to draw conclusions on the clinical hypothetic prognostic value of RN. Thus, we intend to follow our cohort of patients in order to verify this hypothesis.

Concluding, we found evidence of RN atrophy in very early stages of RMS and its association with cerebellar and midbrain WMLV and selective cerebellar lobule atrophy. RN atrophy is worthy of consideration as a promising marker of subclinical cerebellar damage and neurodegeneration in RMS. The prognostic value of RN atrophy merits to be explored given the relative simplicity with which this nucleus can be visualized and measured on routinely available MRI sequences.

DISCLOSURE OF INTERESTS

Monica Margoni reports grants from Genzyme Sanofi, Merck Serono, Biogen Idec, grants and personal fees from Novartis, during the conduct of the study. Sofia Zywicki, Davide Poggiali, Martina Rubin have nothing to disclose. Alice Riccardi reports personal fees from Mylan, Biogen Idec, Genzyme Sanofi. Francesca Rinaldi reports grants and personal fees from Genzyme Sanofi, Merck Serono, Biogen Idec, grants from Novartis, during the conduct of the study. Paola Perini reports grants and personal fees from Merck Serono, Biogen Idec, Genzyme Sanofi, Roche, Novartis, during the conduct of the study. Massimo Filippi is Editor-in-Chief of the Journal of Neurology; received compensation for consulting services and/or speaking activities from Bayer, Biogen Idec, Merck-Serono, Novartis, Roche, Sanofi Genzyme, Takeda, and Teva Pharmaceutical Industries; and receives research support from Biogen Idec, Merck-Serono, Novartis, Roche, Teva Pharmaceutical Industries, Italian Ministry of Health, Fondazione Italiana Sclerosi Multipla, and ARiSLA (Fondazione Italiana di Ricerca per la SLA). Paolo Gallo reports grants and personal fees from Merck Serono, Biogen Idec, Genzyme Sanofi, grants and personal fees from Novartis, grants from University of Padua, Department of Neurosciences DNS, grants from Veneto Region of Italy, grants from Italian Association for Multiple Sclerosis (AISM), grants from Italian Ministry of Public Health, during the conduct of the study.

DATA AVAILABILITY STATEMENT

The data that support the findings of this study are available from the corresponding author upon reasonable request.

ORCID

Monica Margoni https://orcid.org/0000-0002-9232-8964
Massimo Filippi https://orcid.org/0000-0002-5485-0479

REFERENCES

Ashburner, J., & Friston, K. J. (2005). Unified segmentation. *NeuroImage*, *26*(3), 839–851. https://doi.org/10.1016/j.neuroimage.2005.02.018

Avants, B. B., Epstein, C. L., Grossman, M., & Gee, J. C. (2008). Symmetric diffeomorphic image registration with cross-correlation: Evaluating automated labeling of elderly and neurodegenerative brain. *Medical Image Analysis*, *12*(1), 26–41. https://doi.org/10.1016/j.media.2007.06.004

Avants, B. B., Tustison, N. J., Song, G., Cook, P. A., Klein, A., & Gee, J. C. (2011). A reproducible evaluation of ANTs similarity metric performance in brain image registration. *NeuroImage*, *54*(3), 2033–2044. https://doi.org/10.1016/j.neuroimage.2010.09.025

Belhaj-Saif, A., & Cheney, P. D. (2000). Plasticity in the distribution of the red nucleus output to forearm muscles after unilateral lesions of the pyramidal tract. *Journal of Neurophysiology*, *83*(5), 3147–3153. https://doi.org/10.1152/jn.2000.83.5.3147

Colpan, M. E., & Slavin, K. V. (2010). Subthalamic and red nucleus volumes in patients with Parkinson's disease: Do they change with disease progression? *Parkinsonism & Related Disorders*, *16*(6), 398–403. https://doi.org/10.1016/j.parkreldis.2010.03.008

Damasceno, A., Von Glehn, F., Brandao, C. O., Damasceno, B. P., & Cendes, F. (2013). Prognostic indicators for long-term disability in

multiple sclerosis patients. *Journal of the Neurological Sciences*, *324* (1–2), 29–33. https://doi.org/10.1016/j.jns.2012.09.020

D'Ambrosio, A., Pagani, E., Riccitelli, G. C., Colombo, B., Rodegher, M., Falini, A., … Rocca, M. A. (2017). Cerebellar contribution to motor and cognitive performance in multiple sclerosis: An MRI sub-regional volumetric analysis. *Multiple Sclerosis*, *23*(9), 1194–1203. https://doi.org/10.1177/1352458516674567

Eshaghi, A., Prados, F., Brownlee, W. J., Altmann, D. R., Tur, C., Cardoso, M. J., … The MAGNIMS study group. (2018). Deep gray matter volume loss drives disability worsening in multiple sclerosis. *Annals of Neurology*, *83*(2), 210–222. https://doi.org/10.1002/ana.25145

Fischl, B., & Dale, A. M. (2000). Measuring the thickness of the human cerebral cortex from magnetic resonance images. *Proceedings of the National Academy of Sciences of the United States of America*, *97*(20), 11050–11055. https://doi.org/10.1073/pnas.200033797

Habas, C., Guillevin, R., & Abanou, A. (2010). In vivo structural and functional imaging of the human rubral and inferior olivary nuclei: A mini-review. *Cerebellum*, *9*(2), 167–173. https://doi.org/10.1007/s12311-009-0145-1

Keuken, M. C., Bazin, P. L., Backhouse, K., Beekhuizen, S., Himmer, L., Kandola, A., … Forstmann, B. U. (2017). Effects of aging on T(1), T(2)*, and QSM MRI values in the subcortex. *Brain Structure & Function*, *222* (6), 2487–2505. https://doi.org/10.1007/s00429-016-1352-4

Keuken, M. C., Bazin, P. L., Crown, L., Hootsmans, J., Laufer, A., Muller-Axt, C., … Forstmann, B. U. (2014). Quantifying inter-individual anatomical variability in the subcortex using 7 T structural MRI. *NeuroImage*, *94*, 40–46. https://doi.org/10.1016/j.neuroimage.2014.03.032

Koch, M., Mostert, J., Heersema, D., & De Keyser, J. (2007). Tremor in multiple sclerosis. *Journal of Neurology*, *254*(2), 133–145. https://doi.org/10.1007/s00415-006-0296-7

Kochunov, P., Lancaster, J. L., Glahn, D. C., Purdy, D., Laird, A. R., Gao, F., & Fox, P. (2006). Retrospective motion correction protocol for high-resolution anatomical MRI. *Human Brain Mapping*, *27*(12), 957–962. https://doi.org/10.1002/hbm.20235

Koziol, L. F., Budding, D., Andreasen, N., D'Arrigo, S., Bulgheroni, S., Imamizu, H., … Yamazaki, T. (2014). Consensus paper: The cerebellum's role in movement and cognition. *Cerebellum*, *13*(1), 151–177. https://doi.org/10.1007/s12311-013-0511-x

Kurtzke, J. F. (1983). Rating neurologic impairment in multiple sclerosis: An expanded disability status scale (EDSS). *Neurology*, *33*(11), 1444–1452. https://doi.org/10.1212/wnl.33.11.1444

Lang, E. J., Apps, R., Bengtsson, F., Cerminara, N. L., De Zeeuw, C. I., Ebner, T. J., … Xiao, J. (2017). The roles of the Olivocerebellar pathway in motor learning and motor control. A consensus paper. *Cerebellum*, *16*(1), 230–252. https://doi.org/10.1007/s12311-016-0787-8

Lavoie, S., & Drew, T. (2002). Discharge characteristics of neurons in the red nucleus during voluntary gait modifications: A comparison with the motor cortex. *Journal of Neurophysiology*, *88*(4), 1791–1814. https://doi.org/10.1152/jn.2002.88.4.1791

Lazzarotto, A., Margoni, M., Franciotta, S., Zywicki, S., Riccardi, A., Poggiali, D., … Gallo, P. (2020). Selective cerebellar atrophy associates with depression and fatigue in the early phases of relapse-onset multiple sclerosis. *Cerebellum*, *19*(2), 192–200. https://doi.org/10.1007/s12311-019-01096-4

Massion, J. (1988). Red nucleus: Past and future. *Behavioural Brain Research*, *28*(1–2), 1–8. https://doi.org/10.1016/0166-4328(88)90071-x

Onodera, S., & Hicks, T. P. (2009). A comparative neuroanatomical study of the red nucleus of the cat, macaque and human. *PLoS ONE*, *4*(8), e6623. https://doi.org/10.1371/journal.pone.0006623

Parmar, K., Stadelmann, C., Rocca, M. A., Langdon, D., D'Angelo, E., D'Souza, M., … The MAGNIMS study group. (2018). The role of the cerebellum in multiple sclerosis-150 years after Charcot. *Neuroscience and Biobehavioral Reviews*, *89*, 85–98. https://doi.org/10.1016/j.neubiorev.2018.02.012

Philippens, I., Wubben, J. A., Franke, S. K., Hofman, S., & Langermans, J. A. M. (2019). Involvement of the red nucleus in the compensation of parkinsonism may explain why primates can develop stable Parkinson's disease. *Scientific Reports*, *9*(1), 880. https://doi.org/10.1038/s41598-018-37381-1

Polman, C. H., Reingold, S. C., Banwell, B., Clanet, M., Cohen, J. A., Filippi, M., … Wolinsky, J. S. (2011). Diagnostic criteria for multiple sclerosis: 2010 revisions to the McDonald criteria. *Annals of Neurology*, *69*(2), 292–302. https://doi.org/10.1002/ana.22366

Reid, E. K., Norris, S. A., Taylor, J. A., Hathaway, E. N., Smith, A. J., Yttri, E. A., & Thach, W. T. (2009). Is the parvocellular red nucleus involved in cerebellar motor learning? *Current Trends in Neurology*, *3*, 15–22. Retrieved from. https://www.ncbi.nlm.nih.gov/pubmed/21743781

Riccitelli, G., Rocca, M. A., Pagani, E., Rodegher, M. E., Rossi, P., Falini, A., … Filippi, M. (2011). Cognitive impairment in multiple sclerosis is associated to different patterns of gray matter atrophy according to clinical phenotype. *Human Brain Mapping*, *32*(10), 1535–1543. https://doi.org/10.1002/hbm.21125

Schmahmann, J. D., & Sherman, J. C. (1997). Cerebellar cognitive affective syndrome. *International Review of Neurobiology*, *41*, 433–440. https://doi.org/10.1016/s0074-7742(08)60363-3

Schoonheim, M. M., Hulst, H. E., Brandt, R. B., Strik, M., Wink, A. M., Uitdehaag, B. M., … Geurts, J. J. (2015). Thalamus structure and function determine severity of cognitive impairment in multiple sclerosis. *Neurology*, *84*(8), 776–783. https://doi.org/10.1212/WNL.0000000000001285

Siegel, C. S., Fink, K. L., Strittmatter, S. M., & Cafferty, W. B. (2015). Plasticity of intact rubral projections mediates spontaneous recovery of function after corticospinal tract injury. *The Journal of Neuroscience*, *35* (4), 1443–1457. https://doi.org/10.1523/JNEUROSCI.3713-14.2015

Takenobu, Y., Hayashi, T., Moriwaki, H., Nagatsuka, K., Naritomi, H., & Fukuyama, H. (2014). Motor recovery and microstructural change in rubro-spinal tract in subcortical stroke. *NeuroImage: Clinical*, *4*, 201–208. https://doi.org/10.1016/j.nicl.2013.12.003

ten Donkelaar, H. J. (1988). Evolution of the red nucleus and rubrospinal tract. *Behavioural Brain Research*, *28*(1–2), 9–20. https://doi.org/10.1016/0166-4328(88)90072-1

Thompson, A. J., Banwell, B. L., Barkhof, F., Carroll, W. M., Coetzee, T., Comi, G., … Cohen, J. A. (2018). Diagnosis of multiple sclerosis: 2017 revisions of the McDonald criteria. *Lancet Neurology*, *17*(2), 162–173. https://doi.org/10.1016/S1474-4422(17)30470-2

Tintore, M., Rovira, A., Arrambide, G., Mitjana, R., Rio, J., Auger, C., … Montalban, X. (2010). Brainstem lesions in clinically isolated syndromes. *Neurology*, *75*(21), 1933–1938. https://doi.org/10.1212/WNL.0b013e3181feb26f

Triarhou, L. C., Norton, J., & Ghetti, B. (1987). Anterograde transsynaptic degeneration in the deep cerebellar nuclei of Purkinje cell degeneration (pcd) mutant mice. *Experimental Brain Research*, *66*(3), 577–588. https://doi.org/10.1007/BF00270691

Wang, H., & Yushkevich, P. A. (2013). Multi-atlas segmentation with joint label fusion and corrective learning-an open source implementation. *Frontiers in Neuroinformatics*, *7*, 27. https://doi.org/10.3389/fninf.2013.00027

Winkler A.M., Kochunov P, Glahn D.C n.d. *FLAIR Templates*. Retrieved from http://brainder.org.

Yeo, S. S., & Jang, S. H. (2010). Changes in red nucleus after pyramidal tract injury in patients with cerebral infarct. *NeuroRehabilitation*, *27*(4), 373–377. https://doi.org/10.3233/NRE-2010-0622

How to cite this article: Margoni M, Poggiali D, Zywicki S, et al. Early red nucleus atrophy in relapse-onset multiple sclerosis. *Hum Brain Mapp*. 2021;42:154–160. https://doi.org/10.1002/hbm.25213